Research Square

Preprints are preliminary reports that have not undergone peer review.
They should not be considered conclusive, used to inform clinical practice,
or referenced by the media as validated information.

Effects of Climate Change on Hydrogeological Hazard: The Case of the Niscemi Landslides (Southern Sicily, Italy)

Monica Bini

University of Pisa Department of Earth Sciences: Universita degli Studi di Pisa Dipartimento di Scienze della Terra

Marco Luppichini

marco.luppichini@dst.unipi.it

University of Pisa Department of Earth Sciences: Universita degli Studi di Pisa Dipartimento di Scienze della Terra https://orcid.org/0000-0002-0913-3825

Research Article

Keywords: Climate change, Rainfall intensity, Landslide hazard, Mediterranean region, Atmospheric circulation indices

Posted Date: June 5th, 2026

DOI: https://doi.org/10.21203/rs.3.rs-9213751/v1

License: This work is licensed under a Creative Commons Attribution 4.0 International License.
Read Full License

Abstract

This study analyzes precipitation variability and the hydrometeorological conditions associated with extreme hydrogeological events in the Niscemi area (southern Sicily), combining historical series (1885–2020), ERA5 data, and future projections of rainfall intensity.

The comparison between the hydrogeological events of October 12, 1997, and January 26, 2026 highlights how such events can develop through different hydrometeorological configurations, yet are both preceded by high soil moisture conditions, confirming the key role of antecedent precipitation and its temporal distribution.

The climatic analysis shows that cumulative precipitation does not exhibit a significant linear trend but is strongly modulated by Euro-Mediterranean atmospheric circulation, with significant negative correlations with EA (ρ = -0.74) and MOI (ρ = -0.66), and more moderate correlations with NAO and WeMO. In contrast, mean rainfall intensity shows an increasing trend over time and is only weakly correlated with the indices, with a significant relationship observed only with WeMO (ρ = -0.34). The intensification is also associated with synoptic configurations characterized by positive NAO.

Projections obtained using a SARIMAX model, forced with SSP scenarios, indicate a progressive increase in rainfall intensity throughout the 21st century, reaching up to approximately 40% under high-emission scenarios.

Overall, the results highlight that extreme hydrogeological events arise from the interaction between atmospheric circulation variability, thermodynamic conditions, and antecedent rainfall conditions, emphasizing the need for integrated approaches to risk assessment in a climate change context.

2 Introduction

The current climate change is causing a substantial alteration of the hydrological cycle at the global scale (Allen & Ingram, 2002; Bates et al., 2008; Lionello et al., 2017; Trenberth, 2011). In this context, the Mediterranean basin is recognized as one of the primary climate change hotspots, due to its distinctive geographical features and the atmospheric dynamics that characterize it (Giorgi, 2006; Lazoglou et al., 2024). In this region, the effects of global warming are evident in multiple ways.

Among the most significant signals is a progressive intensification of precipitation regimes: on the one hand, a decreasing trend in total annual rainfall is observed (Caporali et al., 2021; Longobardi & Villani, 2010); on the other hand, there is an increase in both the frequency and intensity of extreme events (Libertino et al., 2019; Luppichini et al., 2023; Marani & Zanetti, 2015; Panthou et al., 2014; Ribes et al., 2019; Soldini & Darvini, 2017). At the same time, an increase in the duration and severity of drought periods has been recorded (Baronetti et al., 2022; Guo & Montanari, 2023; Sousa et al., 2011), leading to enhanced soil water stress (Spinoni et al., 2020; S. Vicente-Serrano et al., 2014). This combination of

factors promotes a reduction in infiltration capacity and an intensification of surface runoff processes, thereby amplifying slope instability and hydrogeological hazards (Crozier, 2010; Guzzetti et al., 2007).

The increase in temperature acts as a primary forcing, inducing modifications in atmospheric circulation (Barbero et al., 2018; Berg et al., 2013; Hardwick Jones et al., 2010; Schröer & Kirchengast, 2018), which propagate through cascading effects to territorial impacts. These effects are further modulated and amplified by local morphological and geographical characteristics (Luppichini et al., 2026).

In this context, detailed climate analysis at the local scale remains an open scientific challenge. Although datasets derived from satellite observations (Bruno et al., 2021) and atmospheric reanalysis products (Hersbach et al., 2020) are available, these tools inevitably introduce uncertainties that, at finer spatial scales, may result in significant limitations in the interpretation of climatic signals. The analysis of long-term observed historical series therefore represents a fundamental element in reducing these uncertainties (Luterbacher et al., 2024; Volpi et al., 2024). Italy represents an emblematic case: in addition to its central Mediterranean location, it is among the countries with some of the longest and most continuous climatic time series at the global scale (Brunetti, Maugeri, & Nanni, 2006; Brunetti, Maugeri, Monti, et al., 2006; Luppichini & Bini, 2025; Morbidelli et al., 2025).

However, even in the analysis of observed series, the spatial density of stations and the temporal continuity of measurements play a crucial role. Insufficient or heterogeneous temporal coverage can lead to distorted interpretations of past trends and future projections (Luppichini & Bini, 2025; S. Vicente-Serrano et al., 2025). In a recent study, Luppichini & Bini (2025) analyzed over 100 Italian rainfall series starting from the mid-18th century, highlighting a consistent trend toward increasing intensity of extreme events alongside a decrease in total annual precipitation.

In light of this evidence, the analysis of climate dynamics at the local scale becomes essential to understand the territorial impacts associated with the increasing extremization of precipitation regimes. The increase in rainfall intensity, combined with prolonged drought periods that alter the geotechnical conditions of soils, can enhance slope susceptibility to gravitational instability phenomena (Guzzetti et al., 2007; Peruccacci et al., 2017). The interaction between climatic forcing, lithostratigraphic characteristics, and local morphology is therefore a key factor in the initiation and reactivation of landslides, particularly in areas that are already historically vulnerable (Gariano & Guzzetti, 2016).

A representative case of this dynamic is the urban area of Niscemi (Fig. 1), where the evolution of the climatic framework interacts with predisposing geomorphological conditions, contributing to the reactivation of large-scale instability phenomena.

The urban area of Niscemi has been affected by two major landslide events of significant relevance. The first occurred on October 12, 1997, involving an area of approximately 1.5 km² and causing severe damage to the historic district of Sante Croci, with destruction and uninhabitability of both public and private buildings. The event led to the declaration of a national state of emergency and the activation of

a complex commissioner-based management system, with multi-year funding aimed at slope stabilization, reconstruction, and relocation of buildings (Casagli et al., 2026).

In January 2026, a new phase of instability affected the western and southern margins of the urban area. On January 16, an initial landslide involved the western sector, while on January 25, the 1997 landslide front was reactivated in the southern portion of the town. Overall, the unstable front extends for approximately 4.7 km along the urban edge, with head scarps averaging 25–30 m in height and peaks exceeding 50 m (Fig. 1). The event resulted in a new declaration of a state of emergency (January 26, 2026) and the activation of technical and scientific support structures, requiring a substantial revision of previously planned mitigation measures (Casagli et al., 2026).

This study aims to contextualize, from both a meteorological and climatic perspective, the two main landslide events that have affected the Niscemi area, analyzing their triggering atmospheric factors in light of long-term climate dynamics. The objective is twofold: on the one hand, to reconstruct in detail the rainfall trends in southern Sicily, with particular attention to annual totals, the intensity of extreme events, and their temporal distribution; on the other hand, to assess the future evolution of these variables through the analysis of the Shared Socioeconomic Pathways (SSP) scenarios developed by the IPCC.

The analysis integrates different types of climatic data from heterogeneous databases, combining long-term observed historical series (since the late 19th century) with modern datasets and model outputs. This approach allows the construction of a continuous evolutionary framework linking past climate conditions, present observations, and projections up to 2100.

Through this framework, the study aims to provide a robust and quantitatively grounded assessment of rainfall dynamics in a representative area of the central Mediterranean, with the goal of improving the understanding of the relationships between climate change and the reactivation of slope instability processes.

3 Materials and Methods

3.1 ERA5 Data

The data used in this study were derived from different climatic and meteorological sources. For the detailed meteorological characterization of the two landslide events, hourly data from the ERA5 dataset (ECMWF) were employed, downloaded through the Google Earth Engine platform (https://developers.google.com/earth-engine/datasets/catalog/ECMWF_ERA5_HOURLY). The analyzed variables include total precipitation (total_precipitation), 2 m air temperature (temperature_2m), and volumetric soil water content (volumetric_soil_water_layer_1–4).

Soil moisture is provided for four model layers: 0–7 cm (layer 1), 7–28 cm (layer 2), 28–100 cm (layer 3), and 100–289 cm (layer 4), allowing the assessment of both surface and deeper soil moisture evolution

in the periods preceding the events. ERA5 data are available from January 1, 1940; in this study, they were extracted for the month preceding the events of October 12, 1997, and January 26, 2026, in order to analyze the predisposing meteorological conditions.

To place the events within the climatic context of the most recent three decades, monthly ERA5 data (https://developers.google.com/earth-engine/datasets/catalog/ECMWF_ERA5_MONTHLY) were also used, considering total precipitation and air temperature over the period 1990–2020.

Data extraction was performed for the geographic coordinates 14.391182°E, 37.147382°N (WGS84, EPSG:4326), representative of the study area.

3.2 Measurement data

The study was conducted using validated data from Luppichini and Bini (2025) for the Mineo station (Fig. 1). These data originate from two distinct sources: the first consists of printed volumes published by Filippo Eredia in 1916, and the second is provided by the National System for the Processing and Dissemination of Climate Data (SCIA) of the Italian Institute for Environmental Protection and Research (ISPRA).

The reconstructed monthly time series covers an almost continuous period from 1885 to 2020. From this dataset, monthly cumulative precipitation and the number of rainy days per month were derived, allowing the extraction of an indicator representing rainfall intensity per rainy day. A climatic analysis of these data was carried out, highlighting past variability and long-term trends.

3.3 Climate Indeces Data

To investigate the relationship between precipitation variability and large-scale atmospheric forcing, rainfall time series were compared with several climate teleconnection indices, obtained from official archives and widely used in the international scientific literature. In particular, the Atlantic Multidecadal Oscillation (AMO), the North Atlantic Oscillation (NAO), the East Atlantic pattern (EA), the Western Mediterranean Oscillation (WeMO), and the Mediterranean Oscillation Index (MOI) were considered.

The NAO, in its principal component (PC-based) version, was retrieved from the NCAR Climate Data Guide (https://climatedataguide.ucar.edu/climate-data/hurrell-north-atlantic-oscillation-nao-index-pc-based) and describes variations in sea level pressure differences between Iceland and the Azores, significantly influencing atmospheric circulation over Europe and the Mediterranean basin (Brandimarte et al., 2011; Hurrell, 1995; J.W. Hurrell et al., 2003; Luppichini et al., 2021, 2022; S. M. Vicente-Serrano & López-Moreno, 2008). The EA represents a mode of atmospheric variability similar to the NAO but with centers of action shifted eastward; it exerts a more direct influence on central and southern Europe, modulating storm tracks and precipitation distribution (Halifa-Marín et al., 2025; Luppichini et al., 2022; Mikhailova & Yurovsky, 2016) .

For the Mediterranean context, the WeMO and MOI indices were used, both available from the Climatic Research Unit (CRU; https://crudata.uea.ac.uk/cru/data/moi/). The WeMO is defined based on the

pressure gradient between the Gulf of Cádiz and the Gulf of Genoa and is particularly effective in describing precipitation patterns in the western Mediterranean (Lopez-Bustins et al., 2020; Martin-Vide & Lopez-Bustins, 2006). The MOI, calculated as the normalized difference in sea level pressure between Algiers and Cairo, allows the characterization of internal Mediterranean pressure variability and its implications for regional precipitation regimes (Luppichini et al., 2026).

The statistical relationship between precipitation variables and climate indices was quantified by calculating both the Pearson correlation coefficient (Kirch, 2008), to assess linear relationships, and the Spearman rank correlation coefficient (Spearman, 1904), which is useful for identifying monotonic relationships, including non-linear ones, and is less sensitive to outliers.

The statistical significance of the correlations was evaluated using the corresponding p-values, with results considered statistically significant for p-values lower than 0.05.

3.4 Projections based on IPCC Scenario

The analysis was conducted with the aim of estimating future projections of rainfall intensity based on the observed relationship between temperature and precipitation regime during the historical period.

To this end, for each month, mean rainfall intensity was calculated as the ratio between cumulative precipitation and the number of rainy days (mm/day). The monthly series were then aggregated and reorganized to obtain a continuous time sequence, which was subsequently smoothed using 10-year moving averages in order to reduce interannual variability and highlight decadal-scale components.

Historical temperature data, consistent with the datasets used in IPCC reports and serving as the reference for the construction of the Shared Socioeconomic Pathways (SSP) scenarios, were temporally aligned with the precipitation series.

The statistical relationship between temperature and rainfall intensity was initially assessed using the Spearman correlation coefficient, both on the original and on the filtered series. Subsequently, an autoregressive integrated moving average model with exogenous variables (SARIMAX) was implemented, assuming rainfall intensity as the dependent variable and temperature as the external forcing. The optimal model order (p, d, q) was selected by minimizing the Akaike Information Criterion (AIC), exploring different parameter combinations and evaluating model performance through the coefficient of determination (R^2) and residual analysis.

The model was calibrated over the historical period common to both variables (up to the early 2000s), using normalized anomalies with respect to the 1961–1990 climatological reference period, so as to express the results in percentage terms relative to the climatological mean.

For the forecasting phase, temperature series associated with the SSP1-2.6, SSP2-4.5, SSP3-7.0, and SSP5-8.5 scenarios were concatenated with the historical record and subjected to the same filtering and normalization procedures. The projected temperatures were then used as exogenous input in the

SARIMAX model to estimate the future evolution of rainfall intensity. For each scenario, both the expected mean trajectory and confidence intervals were computed, allowing the quantification of uncertainty associated with the projections.

This approach enables the transfer of the statistical relationship observed in the historical period between temperature and rainfall intensity into the different SSP emission pathways, providing a consistent estimate of the future evolution of precipitation intensity as a function of projected climate warming.

4 Results

4.1 Weather Conditions and Climatic Context

Figure 2 summarizes the reference climatic context and the meteorological conditions associated with the two analyzed events (October 12, 1997, and January 26, 2026), integrating long-term climatology, short-term precipitation dynamics, and antecedent soil moisture conditions through hourly ERA5 data.

Figure 2a shows the monthly distribution of precipitation over the period 1990–2020. The boxplots highlight the pronounced seasonality typical of the Mediterranean climate, with a wet season concentrated in autumn and winter (October–January) and a dry season during late spring and summer (June–August). Mean monthly precipitation frequently exceeds 50–70 mm in autumn, with high interannual variability and the presence of extreme values, particularly in October and November. In contrast, summer months exhibit very low median values (< 10 mm), consistent with prolonged drought conditions. The dashed horizontal lines represent the cumulative precipitation recorded during the months of the two events considered. The January 2026 event (red line) clearly exceeds the monthly climatic median and lies within the upper range of the distribution, indicating exceptionally wet conditions. The October 1997 event (blue line) also falls within the upper portion of the October distribution, consistent with the seasonal peak of autumn precipitation.

Figures 2b and 2d illustrate the hourly evolution of precipitation intensity (blue bars) and volumetric soil water content (green curves) over the 30 days preceding each event. In both cases, the main event was preceded by multiple rainfall episodes that progressively increased soil moisture. For the October 12, 1997 event, a sequence of moderate rainfall in the second half of September led to an increase in soil moisture prior to the main peak. Similarly, the January 26, 2026 event was preceded by a phase of nearly continuous accumulation during the first weeks of January, with already significantly wet soil conditions at the time of the extreme event. In the latter case, a marked increase in water content is also observed in deeper soil layers (layer 3), up to approximately 100 cm, highlighting a progressive wetting process and a more extensive saturation of the soil profile compared to the 1997 event.

Figures 2c and 2e show the cumulative precipitation over the 30 days preceding each event. The 1997 event exhibits a step-like pattern, with significant contributions concentrated in a few intense episodes, for a total of about 100 mm. In contrast, the 2026 event is characterized by a particularly concentrated

accumulation in the last 10 days before the event (approximately 110 mm), within a broader context of total precipitation exceeding 150 mm in the preceding month. This configuration highlights a pronounced pre-saturation condition of the system, with a progressive increase in soil moisture prior to the main rainfall peak.

Overall, the comparison highlights two distinct hydrometeorological configurations. The 2026 event is characterized by a more concentrated precipitation accumulation and a relatively rapid increase in soil moisture in the days immediately preceding the main event. In contrast, the 1997 event developed within a more gradual and temporally distributed accumulation, with a prolonged wetting phase that led to high antecedent saturation conditions prior to the final trigger.

Figure 2 Climatic context and meteorological conditions associated with the events of October 12, 1997, and January 26, 2026. (a) Monthly distribution of precipitation over the reference period 1990–2020; dashed lines indicate the cumulative precipitation recorded during the months of the events. (b, d) Hourly evolution of precipitation (blue bars) and volumetric soil water content (across different layers, layer 1–4, from shallow to deep), with a color scale from green to red indicating increasing depth (layer 1 = green, layer 4 = red) over the 30 days preceding each event; red vertical lines indicate the timing of the main event. (c, e) Cumulative precipitation over the 30 days preceding the events. The comparison highlights different hydrometeorological configurations and antecedent moisture conditions between the two case studies.

Figure 3a shows the monthly distribution of mean temperature over the climatic period 1990–2020. The boxplots highlight the pronounced seasonality typical of the study area, with winter minima in January–February (median values below 10°C) and summer maxima between July and August (medians above 25°C). The dashed lines indicate the mean temperature recorded during the months in which the two events occurred. In both cases, temperatures fall above the 75th percentile of the corresponding monthly distribution.

Figures 3b and 3d show the hourly evolution of temperature over the 30 days preceding each event. For the October 12, 1997 event, a progressive decrease in temperature is observed from the second half of September toward values more typical of early autumn, with a marked daily thermal range. In contrast, the January 26, 2026 event occurs within a fully winter context, characterized by lower temperatures and reduced daily variability compared to the autumn case.

Figures 3c and 3e represent the evolution of mean temperature over the 30 days preceding the events. In 1997, a generally decreasing trend is observed until approximately mid-period, followed by a gradual increase in the days immediately preceding the event. In 2026, temperature shows a rapid drop during the first days of the considered period, followed by a relatively stable phase with slight oscillations around 10–11°C.

Overall, the comparison highlights that the two events occurred under seasonally different thermal conditions: the 1997 case falls within a late summer/early autumn transition phase with still relatively high temperatures, whereas the 2026 event developed under fully winter conditions, with lower

temperatures and greater thermal stability. In both cases, the final rainfall event was preceded by a rapid increase in temperature in the 5–15 days leading up to the event.

4.2 Climate Variability Since 1885 and Its Relationship with Atmospheric Indices

Figure 4 shows the evolution of cumulative monthly precipitation and mean rainfall intensity, both smoothed using a 10-year moving average, together with the main atmospheric circulation indices (NAO, EA, WeMO, and MOI) from 1885 to the present. The use of the moving average highlights decadal and multi-decadal variability, reducing the influence of interannual fluctuations.

Cumulative precipitation exhibits marked oscillations throughout the 20th century, with relatively wet phases between the late 19th and early 20th centuries, a more variable period in the first half of the century, and a drier phase between the 1980s and 1990s. In recent decades, a slight recovery is observed, although no clear monotonic trend emerges across the entire time series. In contrast, mean rainfall intensity shows a more evident increasing trend since the mid-20th century, suggesting a possible reorganization of the precipitation regime, with more intense events on average despite the absence of a comparable increase in total cumulative volumes.

The analysis of atmospheric indices also reveals pronounced multi-decadal variability. The NAO shows alternating positive and negative phases, with a predominantly positive phase in the 1960s–1970s and another in the 1990s, followed by increased variability over the last two decades. The EA index exhibits a prolonged negative phase during the 1960s–1970s, followed by a transition to positive values in the 1980s–1990s, and a persistent positive signal in recent decades. The WeMO shows predominantly positive values in the first half of the 20th century, followed by a progressive shift toward negative values in recent decades. Finally, the MOI displays a marked negative phase in the 1960s–1970s, followed by a positive phase in the 1980s and more moderate oscillations in the recent period.

The visual comparison between rainfall series and atmospheric indices suggests a clear coherence between decadal precipitation variability and index fluctuations. This relationship is confirmed by statistical analysis: cumulative precipitation shows significant negative correlations with EA ($\rho = -0.74$, $p < 0.001$) and MOI ($\rho = -0.66$, $p < 0.001$), as well as more moderate but still significant correlations with NAO ($\rho = -0.30$, $p = 0.005$) and WeMO ($\rho = 0.32$, $p = 0.001$). In particular, positive phases of EA and MOI are associated with reduced cumulative precipitation in the study area, whereas negative phases correspond to relatively wetter periods.

The relationship with rainfall intensity appears weaker and more selective. Only the WeMO shows a significant correlation with intensity ($\rho = -0.34$, $p < 0.001$), while NAO, EA, and MOI do not exhibit robust relationships, except when considering the Pearson coefficient (r) for NAO, which indicates a weak positive correlation with a p-value < 0.05.

	CLIMATE INDEX	Spearman ($\varvec{\rho}$)	$\varvec{p}$	pEARSON ($\varvec{r}$)	$\varvec{p}$
Cumulative Rainfall	NAO	**-0.30**	0.005	**-0.31**	0.004
	WeMO	**0.32**	0.001	**0.41**	< 0.001
	MOI	**-0.66**	< 0.001	**-0.70**	< 0.001
	EA	**-0.74**	< 0.001	**-0.69**	< 0.001
Rainfall Intensity	NAO	0.18	0.107	**0.25**	0.021
	WeMO	**-0.34**	< 0.001	**-0.25**	0.012
	MOI	-0.23	0.104	-0.19	0.193
	EA	-0.18	0.224	-0.14	0.340

4.3 Rainfall intensity projections

Figure 5 shows the projections of anomalies in mean rainfall intensity relative to the reference period 1961–1990, obtained using the SARIMAX model. The model was calibrated on the historical relationship between air temperature and rainfall intensity, accounting for both the internal memory component of the system and the effect of the exogenous variable (temperature). The two variables exhibit a statistically significant correlation, with a Spearman coefficient of 0.47 (p-value < 0.002). The projections were generated using a SARIMAX (1,0,0) model, selected as the optimal configuration based on the AIC criterion and predictive performance, representing the best trade-off between model complexity and explanatory power (R^2 = 0.61 during the calibration period). Future projections were driven by temperature trajectories derived from the SSP1-2.6, SSP2-4.5, SSP3-7.0, and SSP5-8.5 scenarios.

During the historical period (1960–2003), the model reproduces the observed evolution of rainfall intensity consistently (blue line compared to the black line), capturing the main multi-decadal oscillations and the progressive increase observed between the late 1980s and early 2000s. This confirms the robustness of the estimated statistical relationship between temperature and rainfall intensity during the calibration period.

From 2004 onwards, the projections progressively diverge depending on the emission scenario. All scenarios indicate an increase in mean intensity relative to the reference period, with magnitude increasing alongside radiative forcing. In particular: (i) SSP1-2.6 shows a moderate increase that tends to stabilize in the second half of the century, with anomalies between approximately + 15% and + 20% by 2100; (ii) SSP2-4.5 exhibits a more pronounced and continuous increase, reaching values close to + 25% by the end of the century; (iii) SSP3-7.0 and especially SSP5-8.5 display a stronger and more persistent growth, with anomalies exceeding + 35–40% by 2100 under the high-emission scenario.

The shaded bands represent the uncertainty associated with the stochastic component of the model, derived from multiple simulations (ensemble) that account for the system's internal variability. The width of these bands increases over time, reflecting the accumulation of predictive uncertainty over longer time horizons.

5 Discussions

The comparison between the two analysed events highlights how extreme rainfall episodes can develop through different hydrometeorological configurations, while still producing comparable effects in terms of final intensity. The event of October 12, 1997 occurred within a context characterized by a progressive soil wetting phase, driven by moderate precipitation distributed over several preceding weeks. This configuration led to a gradual saturation of the soil profile prior to the main event.

The January 26, 2026 event shows a slightly different dynamic, with rainfall accumulation particularly concentrated in the days immediately preceding the peak and a rapid increase in soil water content. In this case, the hydrological system reached saturation conditions over a relatively short time, suggesting a more prominent role of the temporal clustering of rainfall events in shaping antecedent conditions favorable to triggering the landslide.

These differences indicate that hydrogeological hazard events cannot be interpreted solely as a function of rainfall intensity, but must be analyzed by considering the interaction between precipitation dynamics and antecedent soil moisture conditions (Ozturk et al., 2021; Peruccacci et al., 2017). In both case studies, the main event occurred within a context already characterized by significant water accumulation in the soil–atmosphere system, highlighting the crucial role of antecedent conditions in modulating the hydrological response of the territory.

The analysis of the air temperature shows that both events occurred under relatively high temperature conditions compared to the climatic distribution of the reference month, with values above the 75th percentile. This suggests that anomalous temperature conditions may contribute to the development of intense precipitation by increasing the amount of moisture available in the atmosphere (Arnone et al., 2013; Berg et al., 2013; Pumo et al., 2018).

From a physical perspective, increasing air temperature enhances the atmosphere's capacity to hold water vapor, according to the Clausius–Clapeyron relationship (Pumo et al., 2019; Pumo & Noto, 2021). This implies that, under similar dynamic conditions, warmer air masses can potentially generate more intense precipitation events (Lionello et al., 2006, 2017). The positive correlation observed between temperature and rainfall intensity over the analyzed historical period supports this interpretation, suggesting the existence of a robust statistical link between temperature variability and the intensification of rainfall events.

This behavior is consistent with numerous studies conducted in the Mediterranean basin, where several works have reported an increase in the frequency and intensity of extreme precipitation events in recent

decades (Brunetti, Maugeri, & Nanni, 2006; Park & Min, 2017; Tramblay & Somot, 2018; Trenberth, 2011; Westra et al., 2014). In particular, analyses based on high temporal resolution data have shown that the most significant increases concern short-duration events and the upper tail of the precipitation distribution, while changes in total precipitation are less evident. For example, Treppiedi et al. (2021) showed that many rainfall stations in Sicily exhibit a significant increase in sub-hourly precipitation intensity at higher quantiles, indicating a progressive intensification of the most extreme events despite more limited changes in total rainfall volumes.

The analysis of rainfall series since 1885 highlights how precipitation variability in the study area is strongly influenced by large-scale atmospheric circulation over the Euro-Mediterranean region. Statistically significant correlations between cumulative precipitation and several atmospheric indices indicate that large-scale circulation patterns play a key role in modulating long-term rainfall volumes. Overall, the results suggest that the observed precipitation variability cannot be interpreted as a simple linear trend, but rather reflects multi-decadal oscillations consistent with the different phases of atmospheric circulation indices (Caloiero et al., 2011; Luppichini et al., 2022; Mikhailova & Yurovsky, 2016; Vergni & Chiaudani, 2015; S. M. Vicente-Serrano & López-Moreno, 2008). The modulation exerted by EA and MOI emerges as particularly relevant in controlling precipitation volumes (Luppichini et al., 2026).

These results also indicate that, although the NAO represents one of the main drivers of rainfall variability in the Mediterranean basin, it is not the sole controlling factor of precipitation regimes (Luppichini et al., 2026). Several studies have shown that other atmospheric circulation patterns and regional cyclogenetic processes can play a significant role in modulating Mediterranean precipitation (Lionello et al., 2006; Trigo et al., 2002). In particular, the formation and evolution of Mediterranean cyclonic systems, often associated with local pressure configurations and interactions between air masses of different origins, can favor the development of intense rainfall events even in the absence of strong Atlantic forcing.

In this context, the analysis of synoptic configurations associated with intense precipitation events suggests a relationship with conditions characterized by positive NAO and negative WeMO. This combination tends to shift Atlantic storm tracks toward higher latitudes, reducing the direct contribution of extratropical cyclones over the Mediterranean area (Lopez-Bustins et al., 2020; Martin-Vide & Lopez-Bustins, 2006). At the same time, negative WeMO phases are often associated with pressure configurations that favor moist easterly and south-easterly flows over the western Mediterranean and reduced cyclonic activity in the Gulf of Genoa (Lopez-Bustins et al., 2020; Martin-Vide & Lopez-Bustins, 2006). Under such conditions, mesoscale processes and Mediterranean cyclogenesis become more relevant in driving intense precipitation. Similar synoptic configurations have been observed along the eastern coasts of Spain, where several studies have shown that the most intense rainfall events are frequently associated with the combination of positive NAO and negative WeMO, which promotes the transport of moist Mediterranean air and the development of local convective systems (Lopez-Bustins et al., 2020). This suggests that extreme events in the study area may be influenced by similar atmospheric

dynamics, where reduced Atlantic influence and enhanced Mediterranean cyclogenesis contribute to generating intense and localized precipitation.

These findings fit within a broader context of climate change in the Mediterranean, a region identified as one of the main global climate change hotspots (Giorgi, 2006), characterized by rapid warming and increasing variability of the hydrological cycle. In this context, atmospheric warming and changes in regional circulation may contribute to a reorganization of the precipitation regime, with a tendency toward more intense but often more temporally concentrated events (Caporali et al., 2021; Longobardi & Villani, 2010).

Projections obtained using the SARIMAX model suggest a progressive increase in mean rainfall intensity throughout the 21st century, with magnitude increasing under higher emission scenarios. A key aspect is that, while maintaining internal variability consistent with historical behavior, the mean trajectory of the projections is strongly driven by temperature evolution across the different climate scenarios.

This confirms that, within the estimated model, the increase in rainfall intensity is primarily associated with atmospheric warming, in agreement with the physical expectation related to the increased moisture-holding capacity of warmer air. In other words, the statistical relationship observed between temperature and rainfall intensity in the historical period translates, in future simulations, into a progressive intensification of rainfall events as atmospheric temperature rises.

Overall, the projections suggest that, regardless of the scenario considered, mean rainfall intensity is expected to increase throughout the 21st century, with magnitude proportional to the emission trajectory. High-emission scenarios lead to a stronger acceleration and a wider spread of possible future trajectories, highlighting a potential increase in risk associated with intense rainfall events.

Previous studies based on regional climate model projections suggest a future intensification of extreme precipitation in Sicily, particularly for short-duration events. In this context, the results of this study, indicating a potential increase in rainfall intensity of up to approximately 40% by the end of the 21st century, are consistent with findings from other studies conducted in the Sicilian region (Forestieri et al., 2018). Several studies based on regional climate projections and high-resolution models indicate an increase in extreme precipitation quantiles and an upward shift in depth–duration–frequency (DDF) curves under future scenarios (Forestieri et al., 2018). Similarly, more recent simulations based on convection-permitting climate models and regional projections show an increase in short-duration intense precipitation and its erosivity, as well as a significant rise in extreme quantiles in future DDF curves for Sicily (Buonacera et al., 2025; Dallan et al., 2025). Overall, these results confirm a trend toward intensification of extreme precipitation events in the Mediterranean basin, particularly for short-duration rainfall.

In summary, the results indicate that the generation of extreme events in the study area arises from the interaction of factors operating across different temporal and spatial scales. Large-scale Euro-Mediterranean atmospheric circulation modulates long-term precipitation variability, while favorable

temperature conditions and mesoscale processes contribute to the development of intense rainfall episodes. These atmospheric components are further combined with antecedent soil–atmosphere conditions, which can amplify the hydrological response of the territory during extreme events.

This combination of factors suggests that, under a climate change scenario characterized by higher temperatures and increasing rainfall intensity, events similar to those analyzed may become more frequent or produce more severe impacts. Understanding the mechanisms governing the interaction between climate variability, atmospheric dynamics, and antecedent hydrological conditions is therefore essential to improve risk assessment related to extreme precipitation events.

6 Conclusions

This study analyzed precipitation variability and the hydrometeorological conditions associated with extreme events in the Niscemi area (southern Sicily), combining long-term climatological analyses, assessment of antecedent conditions, and future projections of rainfall intensity.

The comparison between the events of October 12, 1997, and January 26, 2026 highlights how extreme rainfall episodes can develop through different hydrometeorological configurations, yet in both cases are preceded by conditions of high soil moisture. This result underscores the crucial role of antecedent precipitation and the temporal distribution of rainfall events in determining the hydrological response of the territory.

The analysis of the rainfall series since 1885 shows that precipitation variability is strongly modulated by atmospheric circulation at the Euro-Mediterranean scale. In particular, the EA and MOI indices are significantly correlated with cumulative precipitation, indicating that the observed variability reflects multi-decadal oscillations linked to atmospheric circulation dynamics rather than a simple linear trend.

At the same time, mean rainfall intensity shows an increasing trend over time, suggesting a possible reorganization of the precipitation regime, with more intense events on average despite the absence of a similarly evident increase in total precipitation. Furthermore, the analysis highlights that rainfall intensity is associated with synoptic configurations characterized by positive NAO and negative WeMO, conditions that favor a reduced influence of Atlantic disturbances and a greater role of Mediterranean cyclogenetic processes in the development of intense precipitation, as well as air mass advection from east to west across the Mediterranean.

Projections obtained using the SARIMAX model indicate that this trend may continue throughout the 21st century, with rainfall intensity potentially increasing by up to approximately 40% by 2100 under high-emission scenarios. This result is consistent with other projections available for Sicily and with the broader pattern of intensification of extreme precipitation in the Mediterranean under a warming climate.

Overall, the results highlight that extreme rainfall events arise from the interaction between atmospheric circulation variability, thermodynamic conditions, and the antecedent hydrometeorological state of the

territory. In particular, extreme conditions such as prolonged drought periods alternating with intense rainfall events play a key role in modulating hydrological and geomorphological responses, influencing infiltration capacity, surface runoff, and slope susceptibility to landslides. Consequently, future hazard assessment requires an integrated approach that jointly considers atmospheric dynamics and the evolution of soil–atmosphere system conditions.

References

1. Allen, M. R., & Ingram, W. J. (2002). Constraints on future changes in climate and the hydrologic cycle. *Nature*, *419*(6903), 228–232.
2. Arnone, E., Pumo, D., Viola, F., Noto, L. V, & La Loggia, G. (2013). Rainfall statistics changes in Sicily. *Hydrology and Earth System Sciences*, *17*(7), 2449–2458. https://doi.org/10.5194/hess-17-2449-2013
3. Barbero, R., Westra, S., Lenderink, G., & Fowler, H. J. (2018). Temperature-extreme precipitation scaling: a two-way causality? *International Journal of Climatology*, *38*(S1), e1274–e1279. https://doi.org/https://doi.org/10.1002/joc.5370
4. Baronetti, A., Dubreuil, V., Provenzale, A., & Fratianni, S. (2022). Future droughts in northern Italy: high-resolution projections using EURO-CORDEX and MED-CORDEX ensembles. *Climatic Change*, *172*(3), 22. https://doi.org/10.1007/s10584-022-03370-7
5. Bates, B., Kundzewicz, Z., Wu, S., Palutikof, J., & I, I. P. on C. Change. W. G. I. (2008). *Climate change and water*.
6. Berg, P., Moseley, C., & Haerter, J. O. (2013). Strong increase in convective precipitation in response to higher temperatures. *Nature Geoscience*, *6*(3), 181–185.
7. Brandimarte, L., Di Baldassarre, G., Bruni, G., D'Odorico, P., Montanari, A., D'Odorico, P., & Montanari, A. (2011). Relation Between the North-Atlantic Oscillation and Hydroclimatic Conditions in Mediterranean Areas. *Water Resources Management*, *25*(5), 1269–1279. https://doi.org/10.1007/s11269-010-9742-5
8. Brunetti, M., Maugeri, M., Monti, F., & Nanni, T. (2006). Temperature and precipitation variability in Italy in the last two centuries from homogenised instrumental time series. *International Journal of Climatology*, *26*(3), 345–381. https://doi.org/https://doi.org/10.1002/joc.1251
9. Brunetti, M., Maugeri, M., & Nanni, T. (2006). Trends of the daily intensity of precipitation in Italy and teleconnections(*). *IL NUOVO CIMENTO*. https://doi.org/10.1393/ncc/i2005-10227-9
10. Bruno, G., Pignone, F., Silvestro, F., Gabellani, S., Schiavi, F., Rebora, N., Giordano, P., & Falzacappa, M. (2021). Performing Hydrological Monitoring at a National Scale by Exploiting Rain-Gauge and Radar Networks: The Italian Case. *Atmosphere*, *12*(6). https://doi.org/10.3390/atmos12060771
11. Buonacera, G., Palazzolo, N., Cancelliere, A., & Peres, D. J. (2025). Deriving Future Rainfall Depth-Duration-Frequency Curves from Hourly Regional Climate Projections and Simple Scaling in Sicily. *Water Resources Management*, *39*(11), 5619–5635. https://doi.org/10.1007/s11269-025-04219-1

12. Caloiero, T., Coscarelli, R., Ferrari, E., & Mancini, M. (2011). Precipitation change in Southern Italy linked to global scale oscillation indexes. *Nat. Hazards Earth Syst. Sci.*, *11*(6), 1683–1694. https://doi.org/10.5194/nhess-11-1683-2011
13. Caporali, E., Lompi, M., Pacetti, T., Chiarello, V., & Fatichi, S. (2021). A review of studies on observed precipitation trends in Italy. In *International Journal of Climatology* (Vol. 41, Number S1, pp. E1–E25). John Wiley and Sons Ltd. https://doi.org/10.1002/joc.6741
14. Casagli, N., Bianchini, S., Gigli, G., Pazzi, V., Raspini, F., & others. (2026). *Le frane di Niscemi del gennaio 2026. Rapporto n.1*.
15. Crozier, M. J. (2010). Deciphering the effect of climate change on landslide activity: A review. *Geomorphology*, *124*(3), 260–267. https://doi.org/https://doi.org/10.1016/j.geomorph.2010.04.009
16. Dallan, E., Bagarello, V., Ferro, V., Pampalone, V., & Borga, M. (2025). Evaluation and projected changes in rainfall erosivity: Topography dependence revealed by Convection-Permitting climate projections for the Mediterranean island of Sicily. *CATENA*, *254*, 108975. https://doi.org/https://doi.org/10.1016/j.catena.2025.108975
17. Forestieri, A., Arnone, E., Blenkinsop, S., Candela, A., Fowler, H., & Noto, L. V. (2018). The impact of climate change on extreme precipitation in Sicily, Italy. *Hydrological Processes*, *32*(3), 332–348. https://doi.org/https://doi.org/10.1002/hyp.11421
18. Gariano, S. L., & Guzzetti, F. (2016). Landslides in a changing climate. *Earth-Science Reviews*, *162*, 227–252. https://doi.org/https://doi.org/10.1016/j.earscirev.2016.08.011
19. Giorgi, F. (2006). Climate change hot-spots. *Geophysical Research Letters*, *33*(8). https://doi.org/https://doi.org/10.1029/2006GL025734
20. Guo, R., & Montanari, A. (2023). Historical rainfall data in northern Italy predict larger meteorological drought hazard than climate projections. *Hydrology and Earth System Sciences*, *27*(15), 2847–2863. https://doi.org/10.5194/hess-27-2847-2023
21. Guzzetti, F., Peruccacci, S., Rossi, M., & Stark, C. (2007). Rainfall thresholds for the initiation of landslides in Central and Southern Europe. *Meteorology and Atmospheric Physics*, *98*, 239–267. https://doi.org/10.1007/s00703-007-0262-7
22. Halifa-Marín, A., Torres-Vázquez, M. A., Trigo, R., Vicente-Serrano, S. M., Turco, M., Jiménez-Guerrero, P., & Montávez, J. P. (2025). Beyond the NAO: The East Atlantic Pattern's Role in Early 20th-Century Meteorological Droughts in Western Europe. *International Journal of Climatology*. https://doi.org/10.1002/joc.70045
23. Hardwick Jones, R., Westra, S., & Sharma, A. (2010). Observed relationships between extreme sub-daily precipitation, surface temperature, and relative humidity. *Geophysical Research Letters*, *37*(22). https://doi.org/https://doi.org/10.1029/2010GL045081
24. Hersbach, H., Bell, B., Berrisford, P., Hirahara, S., Horányi, A., Muñoz-Sabater, J., Nicolas, J., Peubey, C., Radu, R., Schepers, D., Simmons, A., Soci, C., Abdalla, S., Abellan, X., Balsamo, G., Bechtold, P., Biavati, G., Bidlot, J., Bonavita, M., … Thépaut, J.-N. (2020). The ERA5 global reanalysis. *Quarterly*

Journal of the Royal Meteorological Society, *146*(730), 1999–2049. https://doi.org/https://doi.org/10.1002/qj.3803

25. Hurrell, J. W. (1995). Decadal Trends in the North Atlantic Oscillation: Regional Temperatures and Precipitation. *Science*, *269*(5224), 676 LP – 679-676 LP – 679. https://doi.org/10.1126/science.269.5224.676
26. J.W. Hurrell, Y. Kushnir, G Ottersen, & M Visbeck. (2003). The North Atlantic Oscillation: Climatic Significance and Environmental Impact. *Geophysical Monograph Series*, *84*(8), 73. https://doi.org/10.1029/2003eo080005
27. Kirch, W. (Ed.). (2008). Pearson's Correlation Coefficient. In *Encyclopedia of Public Health* (pp. 1090–1091). Springer Netherlands. https://doi.org/10.1007/978-1-4020-5614-7_2569
28. Lazoglou, G., Papadopoulos-Zachos, A., Georgiades, P., Zittis, G., Velikou, K., Manios, E. M., & Anagnostopoulou, C. (2024). Identification of climate change hotspots in the Mediterranean. *Scientific Reports*, *14*(1), 29817. https://doi.org/10.1038/s41598-024-80139-1
29. Libertino, A., Ganora, D., & Claps, P. (2019). Evidence for Increasing Rainfall Extremes Remains Elusive at Large Spatial Scales: The Case of Italy. *Geophysical Research Letters*, *46*(13), 7437–7446. https://doi.org/https://doi.org/10.1029/2019GL083371
30. Lionello, P., Malanotte-Rizzoli, P., Boscolo, R., Alpert, P., Artale, V., Li, L., Luterbacher, J., Trigo, R., Tsimplis, M., Ulbrich, U., & Xoplaki, E. (2006). The Mediterranean Climate: An Overview of the Main Characteristics and Issues. *Developments in Earth and Environmental Sciences*, *4*, 1–26. https://doi.org/10.1016/S1571-9197(06)80003-0
31. Lionello, P., Özsoy, E., Planton, S., & Zanchetta, G. (2017). Climate Variability and Change in the Mediterranean Region. *Global and Planetary Change*, *151*, 1–3. https://doi.org/10.1016/j.gloplacha.2017.04.005
32. Longobardi, A., & Villani, P. (2010). Trend analysis of annual and seasonal rainfall time series in the Mediterranean area. *International Journal of Climatology*, *30*(10), 1538–1546. https://doi.org/https://doi.org/10.1002/joc.2001
33. Lopez-Bustins, J. A., Arbiol-Roca, L., Martin-Vide, J., Barrera-Escoda, A., & Prohom, M. (2020). Intra-annual variability of the Western Mediterranean Oscillation (WeMO) and occurrence of extreme torrential precipitation in Catalonia (NE Iberia). *Natural Hazards and Earth System Sciences*, *20*(9), 2483–2501. https://doi.org/10.5194/nhess-20-2483-2020
34. Luppichini, M., Barsanti, M., Giannecchini, R., & Bini, M. (2021). Statistical relationships between large-scale circulation patterns and local-scale effects: NAO and rainfall regime in a key area of the Mediterranean basin. *Atmospheric Research*, *248*, 105270. http://www.sciencedirect.com/science/article/pii/S0169809520312072
35. Luppichini, M., & Bini, M. (2025). Evolution of rainfall in Italy over the last 200 years: Interactions between climate indices and global warming. *Atmospheric Research*, *326*. https://doi.org/10.1016/j.atmosres.2025.108276

36. Luppichini, M., Bini, M., Barsanti, M., Giannecchini, R., & Zanchetta, G. (2022). Seasonal rainfall trends of a key Mediterranean area in relation to large-scale atmospheric circulation: How does current global change affect the rainfall regime? *Journal of Hydrology*, *612*, 128233. https://doi.org/https://doi.org/10.1016/j.jhydrol.2022.128233
37. Luppichini, M., Bini, M., Giannecchini, R., & Zanchetta, G. (2023). High-resolution spatial analysis of temperature influence on the rainfall regime and extreme precipitation events in north-central Italy. *Science of The Total Environment*, *880*, 163368. https://doi.org/https://doi.org/10.1016/j.scitotenv.2023.163368
38. Luppichini, M., Natali, S., Columbu, A., Zanchetta, G., & Bini, M. (2026). Mediterranean precipitation variability is driven by complex atmospheric mechanisms beyond the North Atlantic Oscillation. *Communications Earth & Environment*. https://doi.org/10.1038/s43247-025-03104-4
39. Luterbacher, J., Allan, R., Wilkinson, C., Hawkins, E., Teleti, P., Lorrey, A., Brönnimann, S., Hechler, P., Velikou, K., & Xoplaki, E. (2024). The Importance and Scientific Value of Long Weather and Climate Records; Examples of Historical Marine Data Efforts across the Globe. *Climate*, *12*(3). https://doi.org/10.3390/cli12030039
40. Marani, M., & Zanetti, S. (2015). Long-term oscillations in rainfall extremes in a 268 year daily time series. *Water Resources Research*, *51*(1), 639–647. https://doi.org/https://doi.org/10.1002/2014WR015885
41. Martin-Vide, J., & Lopez-Bustins, J.-A. (2006). The Western Mediterranean Oscillation and rainfall in the Iberian Peninsula. *International Journal of Climatology*, *26*(11), 1455–1475. https://doi.org/https://doi.org/10.1002/joc.1388
42. Mikhailova, N., & Yurovsky, A. (2016). The East Atlantic Oscillation: Mechanism and Impact on the European Climate in Winter. *Physical Oceanography*. https://doi.org/10.22449/1573-160X-2016-4-25-33
43. Morbidelli, R., Flammini, A., Echeta, O., Albano, R., Anzolin, G., Zumr, D., Badi, W., Berni, N., Bertola, M., Bodoque, J., Brandsma, T., Cauteruccio, A., Cesanelli, A., Cimorelli, L., Chaffe, P., Chagas, V., Dari, J., Almeida, C., Díez-Herrero, A., & Saltalippi, C. (2025). A reassessment of the history of the temporal resolution of rainfall data at the global scale. *Journal of Hydrology*, *654*, 132841. https://doi.org/10.1016/j.jhydrol.2025.132841
44. Ozturk, U., Pittore, M., Behling, R., Roessner, S., Andreani, L., & Korup, O. (2021). How robust are landslide susceptibility estimates? *Landslides*, *18*(2), 681–695. https://doi.org/10.1007/s10346-020-01485-5
45. Panthou, G., Mailhot, A., Laurence, E., & Talbot, G. (2014). Relationship between surface temperature and extreme rainfalls: A multi-time-scale and event-based analysis. *Journal of Hydrometeorology*, *15*(5), 1999–2011.
46. Park, I. H., & Min, S. K. (2017). Role of convective precipitation in the relationship between subdaily extreme precipitation and temperature. *Journal of Climate*, *30*(23), 9527–9537. https://doi.org/10.1175/JCLI-D-17-0075.1

47. Peruccacci, S., Brunetti, M. T., Gariano, S. L., Melillo, M., Rossi, M., & Guzzetti, F. (2017). Rainfall thresholds for possible landslide occurrence in Italy. *Geomorphology*, *290*, 39–57. https://doi.org/https://doi.org/10.1016/j.geomorph.2017.03.031
48. Pumo, D., Carlino, G., Arnone, E., & Noto, L. V. (2018). Relationship between extreme rainfall and surface temperature in Sicily (Italy). *EPiC Series in Engineering*, *3*, 1718–1726.
49. Pumo, D., Carlino, G., Blenkinsop, S., Arnone, E., Fowler, H., & Noto, L. V. (2019). Sensitivity of extreme rainfall to temperature in semi-arid Mediterranean regions. *Atmospheric Research*, *225*, 30–44. https://doi.org/https://doi.org/10.1016/j.atmosres.2019.03.036
50. Pumo, D., & Noto, L. V. (2021). Exploring the linkage between dew point temperature and precipitation extremes: A multi-time-scale analysis on a semi-arid Mediterranean region. *Atmospheric Research*, *254*, 105508. https://doi.org/https://doi.org/10.1016/j.atmosres.2021.105508
51. Ribes, A., Thao, S., Vautard, R., Dubuisson, B., Somot, S., Colin, J., Planton, S., & Soubeyroux, J.-M. (2019). Observed increase in extreme daily rainfall in the French Mediterranean. *Climate Dynamics*, *52*(1), 1095–1114.
52. Schröer, K., & Kirchengast, G. (2018). Sensitivity of extreme precipitation to temperature: the variability of scaling factors from a regional to local perspective. *Climate Dynamics*, *50*(11), 3981–3994.
53. Soldini, L., & Darvini, G. (2017). Extreme rainfall statistics in the Marche region, Italy. *Hydrology Research*, *48*(3), 686–700. https://doi.org/10.2166/nh.2017.091
54. Sousa, P. M., Trigo, R. M., Aizpurua, P., Nieto, R., Gimeno, L., & Garcia-Herrera, R. (2011). Trends and extremes of drought indices throughout the 20th century in the Mediterranean. *Natural Hazards and Earth System Sciences*, *11*(1), 33–51. https://doi.org/10.5194/nhess-11-33-2011
55. Spearman, C. (1904). The proof and measurement of association between two things. *The American Journal of Psychology*, *15*(1), 72–101. https://doi.org/10.2307/1412159
56. Spinoni, J., Barbosa, P., Bucchignani, E., Cassano, J., Cavazos, T., Christensen, J. H., Christensen, O. B., Coppola, E., Evans, J., Geyer, B., Giorgi, F., Hadjinicolaou, P., Jacob, D., Katzfey, J., Koenigk, T., Laprise, R., Lennard, C. J., Kurnaz, M. L., Li, D., … Dosio, A. (2020). Future Global Meteorological Drought Hot Spots: A Study Based on CORDEX Data. *Journal of Climate*, *33*(9), 3635–3661. https://doi.org/https://doi.org/10.1175/JCLI-D-19-0084.1
57. Tramblay, Y., & Somot, S. (2018). Future evolution of extreme precipitation in the Mediterranean. *Climatic Change*, *151*(2), 289–302. https://doi.org/10.1007/s10584-018-2300-5
58. Trenberth, K. E. (2011). Changes in precipitation with climate change. *Climate Research*, *47*(1–2), 123–138. https://www.int-res.com/abstracts/cr/v47/n1-2/p123-138/
59. Treppiedi, D., Cipolla, G., Francipane, A., & Noto, L. V. (2021). Detecting precipitation trend using a multiscale approach based on quantile regression over a Mediterranean area. *International Journal of Climatology*, *41*(13), 5938–5955. https://doi.org/10.1002/joc.7161

60. Trigo, I. F., Bigg, G. R., & Davies, T. D. (2002). *Climatology of Cyclogenesis Mechanisms in the Mediterranean*.
61. Vergni, L., & Chiaudani, A. (2015). *Relationship between the NAO index and some indices of extreme precipitation in the Abruzzo Region*. http://climatedataguide.ucar.edu/guidance/hurrell-north-
62. Vicente-Serrano, S., López-Moreno, J. I., Beguería, S., Lorenzo-Lacruz, J., Sanchez-Lorenzo, A., García-Ruiz, J. M., Azorin-Molina, C., Morán-Tejeda, E., Revuelto, J., Trigo, R., Coelho, M. F., & Espejo, F. (2014). Evidence of increasing drought severity caused by temperature rise in southern Europe. *Environmental Research Letters*, *9*, 044001.
63. Vicente-Serrano, S. M., & López-Moreno, J. I. (2008). Nonstationary influence of the North Atlantic Oscillation on European precipitation. *Journal of Geophysical Research: Atmospheres*, *113*(D20). https://doi.org/10.1029/2008JD010382
64. Vicente-Serrano, S., Tramblay, Y., Reig Gracia, F., Gonzalez-Hidalgo, J., Beguería, S., Brunetti, M., Cindric Kalin, K., Patalen, L., Kržič, A., Lionello, P., Lima, M., Trigo, R., Kenawy, A., Eddenjal, A., Türkeş, M., Koutroulis, A., Manara, V., Maugeri, M., Badi, W., & Potopová, V. (2025). High temporal variability not trend dominates Mediterranean precipitation. *Nature*, *639*, 658–666. https://doi.org/10.1038/s41586-024-08576-6
65. Volpi, E., Mancini, C. P., & Fiori, A. (2024). What can we learn from long hydrological time-series? The case of rainfall data at Collegio Romano, Rome, Italy. *Journal of Hydrology X*, *23*, 100176. https://doi.org/https://doi.org/10.1016/j.hydroa.2024.100176
66. Westra, S., Fowler, H. J., Evans, J. P., Alexander, L. V, Berg, P., Johnson, F., Kendon, E. J., Lenderink, G., & Roberts, N. (2014). Future changes to the intensity and frequency of short-duration extreme rainfall. *Reviews of Geophysics*, *52*(3), 522–555.

Figures

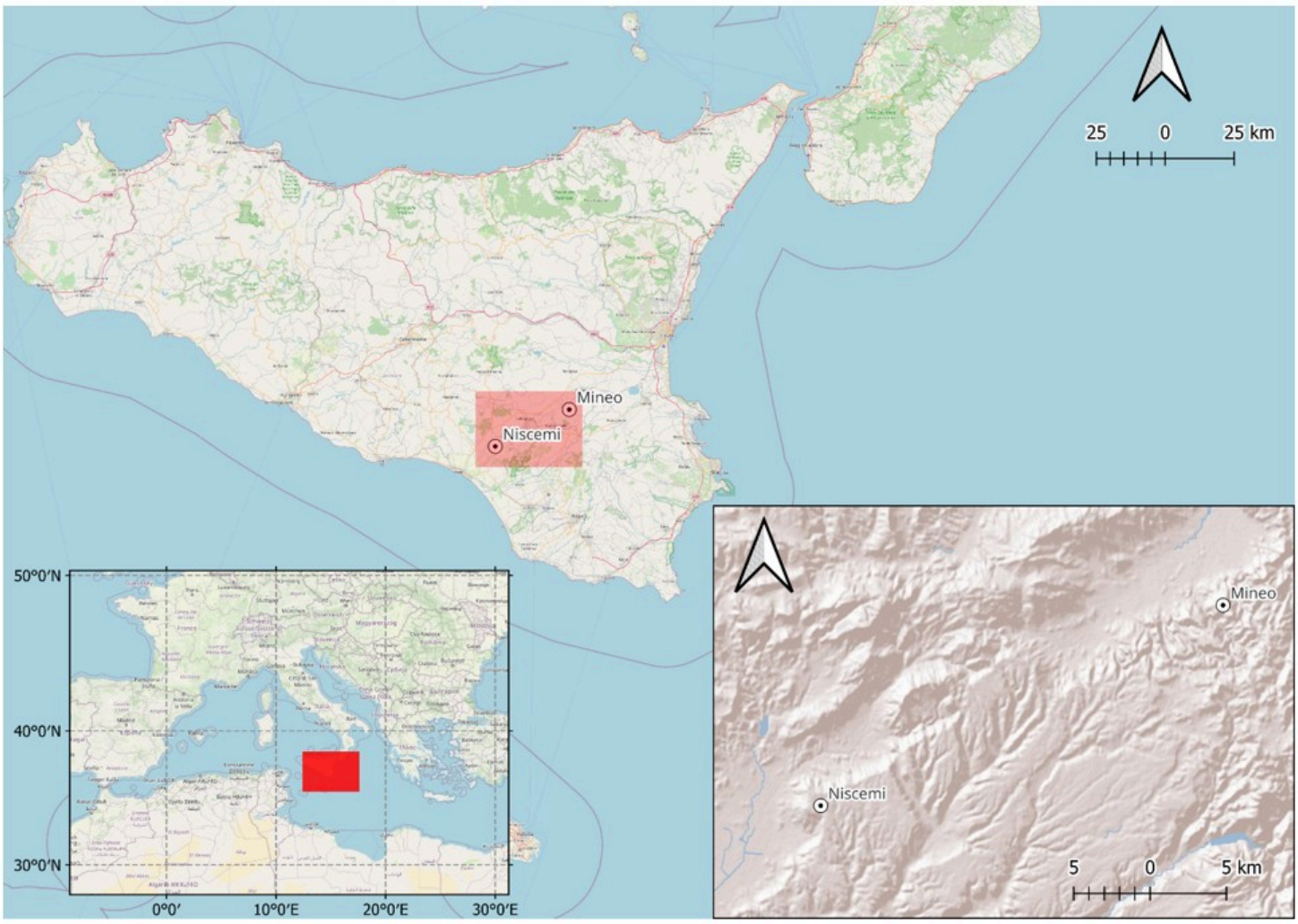


Figure 1

Study Area

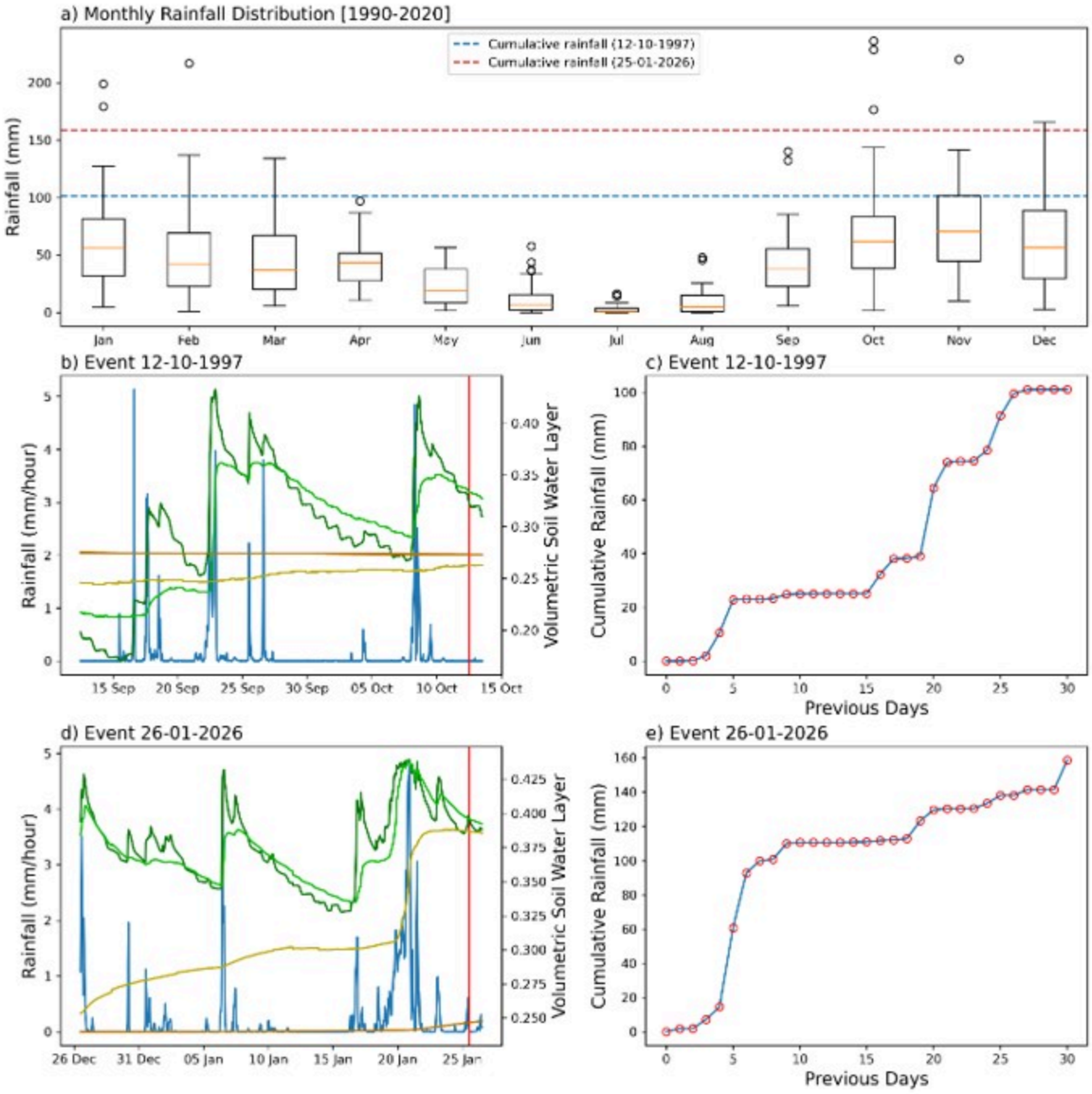


Figure 2

Climatic context and meteorological conditions associated with the events of October 12, 1997, and January 26, 2026. (a) Monthly distribution of precipitation over the reference period 1990–2020; dashed lines indicate the cumulative precipitation recorded during the months of the events. (b, d) Hourly evolution of precipitation (blue bars) and volumetric soil water content (across different layers, layer 1–4, from shallow to deep), with a color scale from green to red indicating increasing depth (layer 1 = green, layer 4 = red) over the 30 days preceding each event; red vertical lines indicate the timing of the main event. (c, e) Cumulative precipitation over the 30 days preceding the events. The comparison highlights

different hydrometeorological configurations and antecedent moisture conditions between the two case studies.

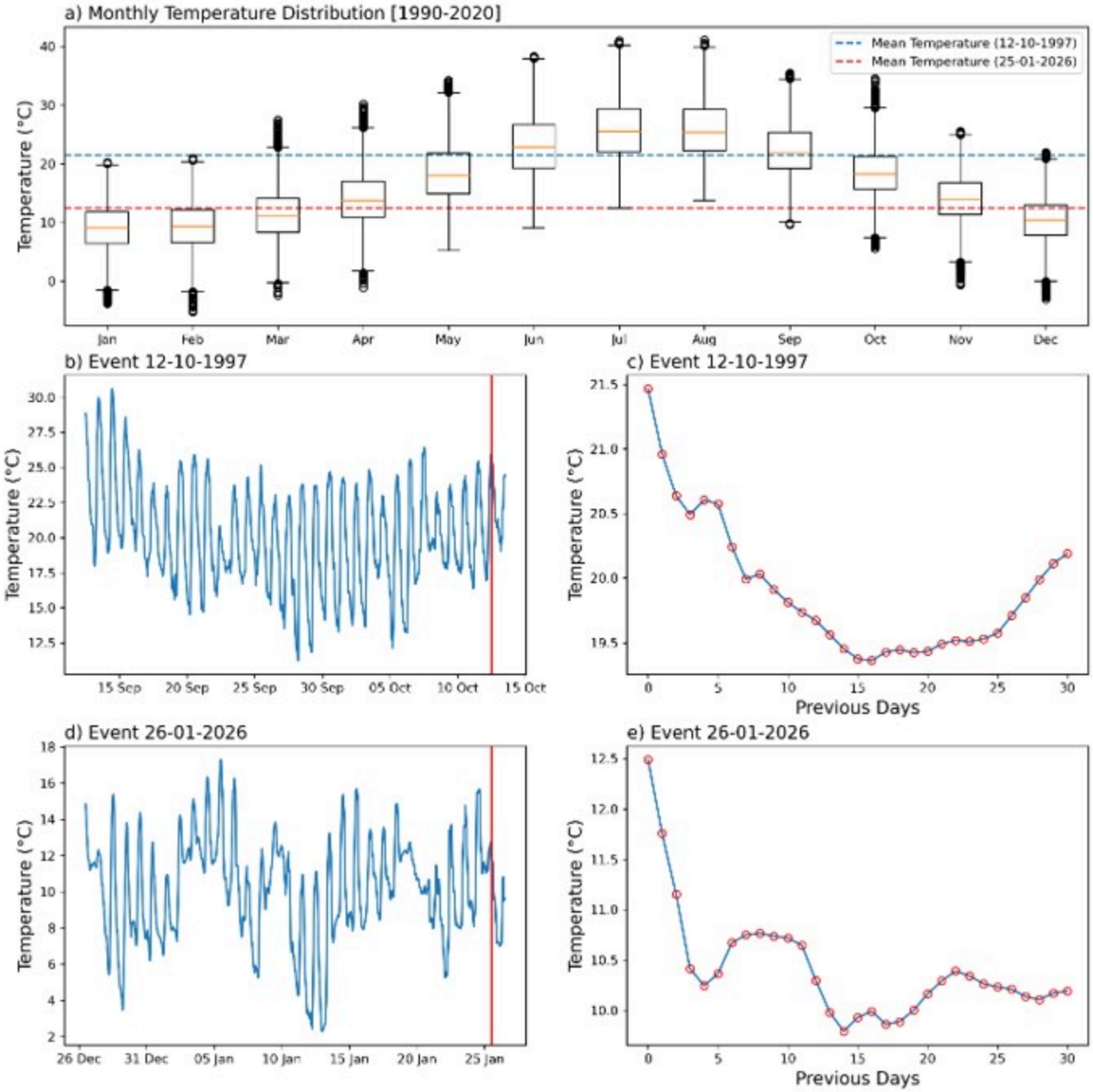


Figure 3

Climatic context and meteorological conditions associated with the events of October 12, 1997, and January 26, 2026. (a) Monthly distribution of temperature over the reference period 1990–2020; dashed lines indicate the mean temperature recorded on the day of the events. (b, d) Hourly evolution of temperature (blue bars) over the 30 days preceding each event; red vertical lines indicate the timing of the main event. (c, e) Mean temperature over the 30 days preceding the events.

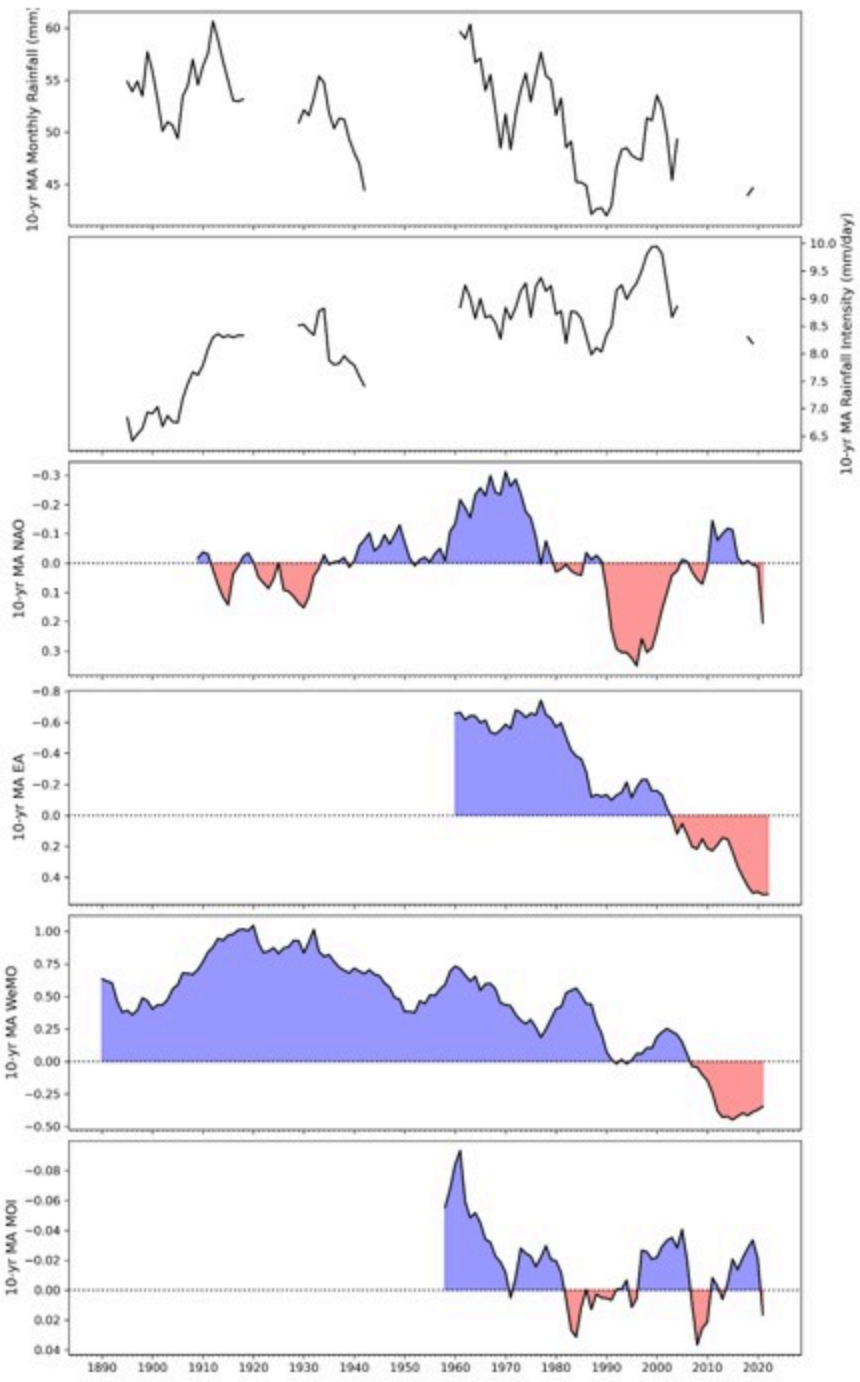


Figure 4

Long-period rainfall analysis for the stations in Mineo and Atmospheric teleconnection index

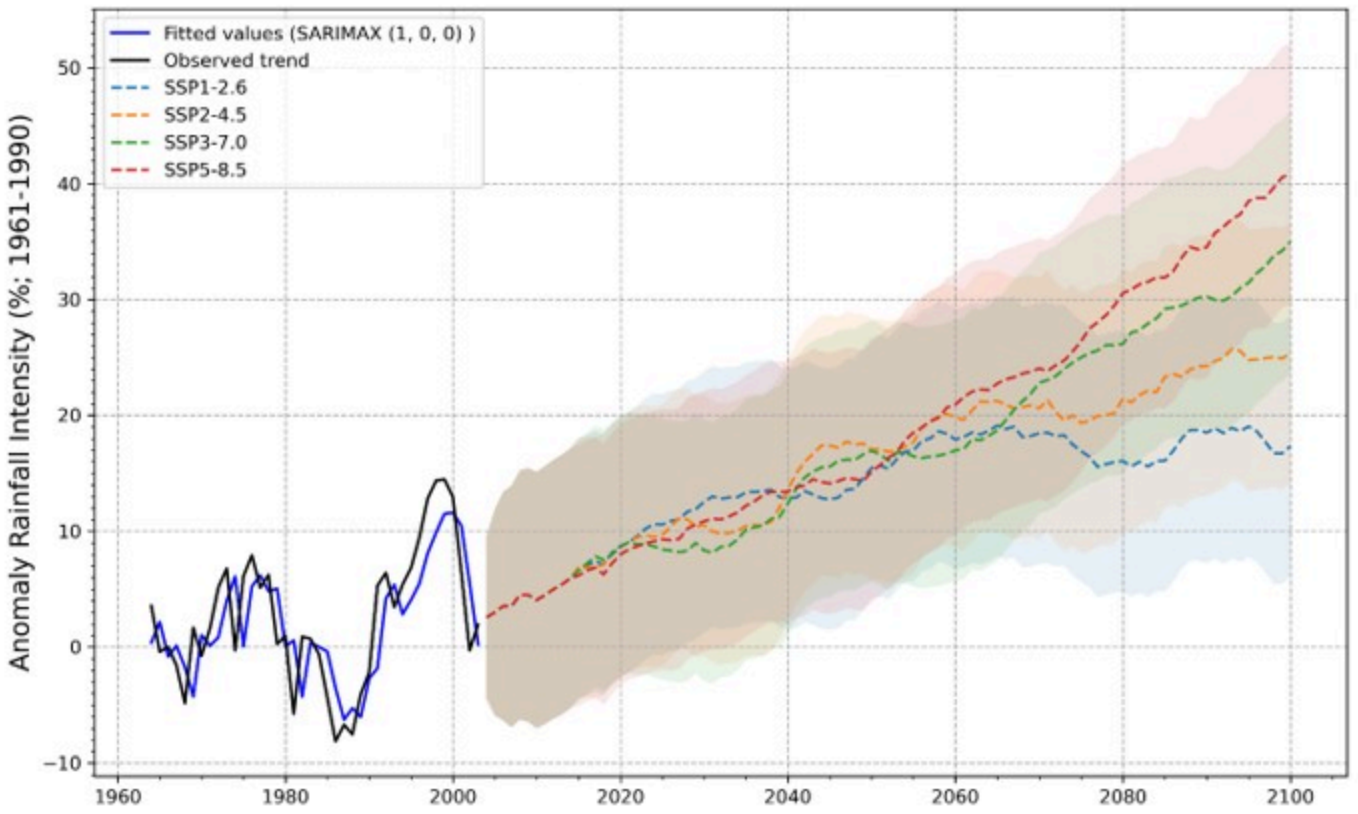


Figure 5

Projected anomalies of mean rainfall intensity (%) relative to the 1961–1990 reference period, obtained using the SARIMAX (1,0,0) model forced by temperature projections under different SSP scenarios. The black line represents the observed trend, while the blue line shows the model fit over the historical calibration period. Future projections (2004–2100) are shown for SSP1-2.6 (blue dashed), SSP2-4.5 (orange dashed), SSP3-7.0 (green dashed), and SSP5-8.5 (red dashed). Shaded areas indicate the 90% confidence intervals associated with the model ensemble.